SCIENCE CHINA PRESS

SCIENCE CHINA Chemistry 2026 69(11): 6273–6278
https://doi.org/10.1007/s11426-026-3647-6

SPECIAL TOPIC: Nucleic Acid Nanotechnology

ARTICLES

Light-controlled DNA nanomotors for programmable intracellular transport in synthetic cell-like droplets

Danlong Chen[1,2], Yunxiao Wang[1], Shijun Xu[1], Fan Xia[1] & Fujian Huang[1*]

[1]State Key Laboratory of Geomicrobiology and Environmental Changes, Faculty of Materials Science and Chemistry, China University of Geosciences, Wuhan 430074, China
[2]Jiaxing Key Laboratory of Biosemiconductors, Xiangfu Laboratory, Jiashan 314102, China
*Corresponding author (email: huangfj@cug.edu.cn)

Received 20 April 2026; Accepted 8 June 2026; Published online 22 September 2026

Abstract Intracellular transport, essential for cellular function, is driven by biomolecular motors moving along cytoskeletal networks. While *in vitro* models have advanced our understanding, replicating the versatility and controllability of native intracellular transport remains challenging. Here, we report a synthetic cell-like model equipped with a light-controlled DNA-based motor capable of light-guided transport along an artificial DNA cytoskeleton. The system consists of self-assembled DNA fibers serving as structural scaffolds and RNA hairpins functionalized with a photocleavable linker (PC-linker) as motor tracks. Upon UV (ultraviolet) irradiation, the motors conjugated to SUV (small unilamellar vesicle) or nanoparticles are activated via strand displacement and RNase H-mediated hydrolysis, enabling directional motion along the fiber axis. Encapsulated within water-in-oil emulsion droplets to mimic cellular confinement, these synthetic cell-like droplets allow spatiotemporally controlled SUV transport using light. This programmable and biocompatible platform offers a robust model for studying subcellular dynamics and paves the way for advanced synthetic biology applications.

Keywords DNA motors, photoresponsive DNA/RNA, DNA fiber skeleton, synthetic cell-like droplets

1 Introduction

In living cells, the precise and efficient transport of substances is fundamental to maintaining vital biological activities. This process is orchestrated by a sophisticated intracellular network composed of cytoskeletal elements such as microtubules and microfilaments, which serve as tracks for biomolecular motors. These motors, including kinesin and dynein proteins, facilitate the directed movement of vesicles, organelles, and other cargo to specific locations within the cell [1,2]. For instance, vesicles derived from the endoplasmic reticulum are transported along microtubules to the Golgi apparatus, a process requiring both spatial precision and kinetic efficiency [3,4].

Recent advances in DNA nanotechnology have enabled the development of synthetic molecular motors-DNA-based nanomotors-that emulate the functions of their biological counterparts [5–11]. DNA nanomotors are programmable nanoscale devices capable of directional movement along predefined DNA tracks, powered by chemical energy sources such as ATP or light [12,13]. Compared to natural motor proteins, DNA motors offer several distinct advantages: their motion can be precisely controlled through sequence design, allowing customization of speed, direction, and pathway [14–18]; they operate with high precision at the nanoscale; and they exhibit excellent biocompatibility and biodegradability, making them promising for biomedical applications [19–22]. These attributes make DNA motors particularly attractive for integration into synthetic cells-artificial systems designed to mimic the structure and functionality of natural cells [23,24]. Incorporating DNA motors into such constructs enables programmable control over intracellular transport, offering novel opportunities to study subcellular dynamics, detect biomarkers, and develop functional bionanodevices [25–28]. In recent years, researchers have attempted to construct DNA-based motors within synthetic cells. Zhan *et al.* [29] utilized a DNA skeleton and an RNase H-driven "burnt-bridge" mechanism to achieve guided movement of lipid vesicles along DNA filaments inside artificial cells. Chen *et al.* [30] developed a DNA reaction network as a feed-forward control center to enable dynamic self-assembly and multilayered hierarchical assembly of DNA nanotubes in artificial cells, and further employed this artificial cytoskeleton to restrict the motion of artificial motors. Moreover, Ramos Docampo *et al.* [31] used nanomotors surface-modified with the actin-polymerizing protein ActA to polymerize actin *in situ* within the lumen of artificial cells, thereby forming a semi-synthetic cytoskeletal network.

Despite the above-mentioned work demonstrating the initial integration of artificial cytoskeletons and transport functions, the deployment of DNA motors inside confined cell-like compartments remains underexplored, and their operational stability, loading versatility, and compatibility with synthetic cellular architectures constitute significant translational bottlenecks. Light-responsive molecular systems represent a particularly promising avenue for overcoming these limitations. Light, as a non-invasive and spatiotemporally precise stimulus, provides an ideal means to regulate motor activity [32–35]. Photoresponsive mechanisms have been increasingly employed in biomedicine and nanotechnology to achieve high-resolution control over molecular processes [36–39]. Photocontrol enables non-invasive and finely localized activation, making it ideal for regulating dynamics in emulsion-based or lipid-bound synthetic cells. However, integrating photochemical triggers with DNA-based nanostructures that function

Citation: Chen D, Wang Y, Xu S, Xia F, Huang F. Light-controlled DNA nanomotors for programmable intracellular transport in synthetic cell-like droplets. *Sci China Chem*, 2026, 69: 6273–6278. https://doi.org/10.1007/s11426-026-3647-6

https://www.sciengine.com/doi/10.1007/s11426-026-3647-6

© Science China Press 2026

reliably under physiological conditions requires sophisticated design strategies to prevent premature activation, ensure efficient coupling with enzymatic drivers, and maintain motion consistency across heterogeneous environments. In this work, we address these challenges through the development of a programmable synthetic cell-like system featuring a photoresponsive DNA motor operating on an artificial cytoskeleton. Our design combines structural DNA fibers with photoactivatable RNA tracks to achieve RNase H-powered directional transport of diverse cargoes, from SUV to inorganic nanoparticles, within water-in-oil emulsion droplets that mimic cellular confinement. Our approach combines programmable DNA architecture with photochemical triggering to emulate and investigate controlled intracellular transport in a confined biomimetic environment. By demonstrating photoresponsive control over motor behavior at the single-synthetic-cell level, we not only overcome key limitations of existing synthetic transport systems but also establish a robust and scalable architecture for future applications in targeted delivery, diagnostic probing, and adaptive biomaterial design. Compared with existing DNA walkers, most of which require periodic fuel addition or rely on diffusive motion and thus lack autonomy and spatial controllability, the light-responsive DNA motor described here utilizes RNase H-driven hydrolysis to achieve autonomous and processive walking, along with UV-light-triggered on-demand activation with spatial precision. Moreover, most existing synthetic cell systems depend on diffusion or external fields (*e.g.*, magnetic fields). In this work, we construct linear directional transport along a DNA fiber scaffold within cell-sized confined compartments and demonstrate that SUVs can be recruited to a specific illuminated region, thereby mimicking intracellular transport along the cytoskeleton. This platform bridges critical gaps between nucleic acid nanotechnology and synthetic cell development, offering a new paradigm for designing intelligent cellular mimics with advanced transport functionalities. Its modular nature and biocompatibility further suggest strong potential for eventual deployment in biohybrid systems and therapeutic applications, paving the way for a new generation of dynamic artificial cells.

2 Results and discussion

2.1 Light-controlled locomotion mechanism of DNA nanomotors on artificial cytoskeletal fibers

As illustrated in Figure 1, the locomotion of DNA nanomotors along artificial cytoskeletal fibers is driven by a light-triggered, RNase H-mediated mechanism. Each motor consists of a single-stranded Walker DNA conjugated to the SUV surface and a photocleavable 2-nitrobenzyl linker (PC-linker) integrated into a track assembly, forming a light-responsive DNA-RNA complex. The track nucleic acid includes a single-stranded DNA segment (tail a2) and a photoresponsive RNA hairpin, which is anchored to the fiber skeleton via base pairing between fragment a1 and DNA tail a2. Under UV irradiation, the PC-linker cleaves, activating the RNA hairpin and initiating a toehold-mediated strand displacement reaction with the Walker DNA. This results in the formation of an RNA/DNA heteroduplex, which is subsequently hydrolyzed by RNase H, releasing the Walker DNA and enabling it to engage in further hybridization cycles. The chemical energy derived from this process is converted into kinetic energy, propelling the SUV unidirectionally along the fiber track. This mechanism resembles the "burnt-bridge Brownian ratchet" model, ensuring progressive motion toward new binding sites on the track RNA [40–42].

2.2 Design and characterization of DNA synthetic cytoskeleton

The artificial cytoskeleton was constructed via self-assembly of five distinct single-stranded DNAs into micron-scale hollow fiber structures (DNA tiles) (Figure 2a). Each tile features four sticky ends that facilitate inter-tile interactions, leading to the formation of tubular fibers with a circumference of 6–8 tiles (sequences provided in Table S1, Supporting Information online) [43]. Gel electrophoresis confirmed successful hybridization and fiber formation (Figure S1, Supporting Information online). Scanning electron microscopy (SEM) revealed well-defined fibrous morphologies (Figure 2b), and confocal imaging of Cy5-labeled fibers further validated their structural integrity, with an average length of approximately 3.5 μm (Figure 2c, d). Self-assembly conditions, including strand concentration, buffer composition, Mg^{2+} concentration, and pH, were systematically optimized to enhance fiber yield and length. Mg^{2+} concentration proved particularly critical, with higher concentrations promoting fiber formation and structural uniformity (Figures S2–S5). The finally optimized self-assembly conditions for the DNA fibers are as follows: every single strand at an equimolar concentration of 5 μM in Tris-acetate-EDTA (TAE) buffer (pH 8.0) containing 150 mM NaCl and 15 mM $MgCl_2$, with an annealing program of heating at 95 °C for 10 min followed by slow cooling to

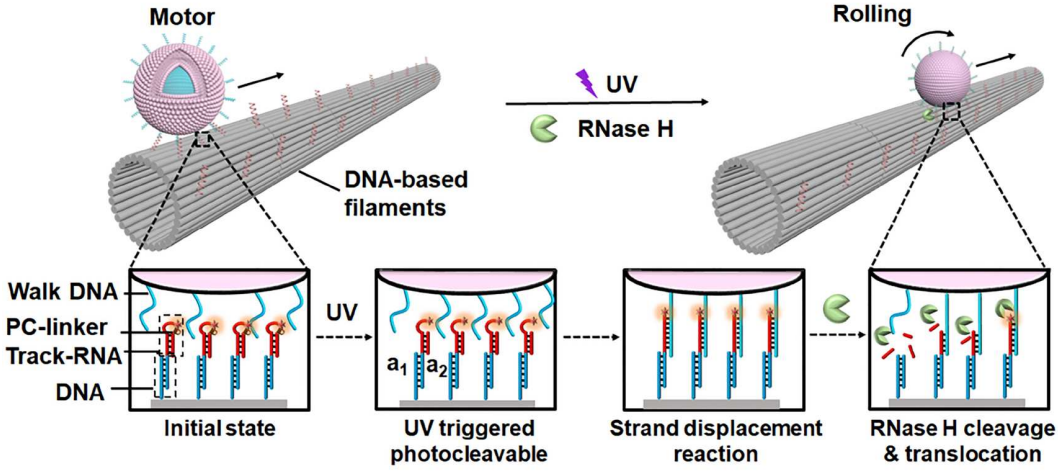

Figure 1 (Color online) Schematic illustration of the light-controlled walking of nanoscale nucleic acid motors on DNA fiber assemblies. The processes of binding and hydrolysis of the DNA motor on the DNA fiber structure are shown. The motor attaches to the DNA filament and achieves directional movement through specific nucleic acid sequences. The enlarged inset shows the initial state of the DNA motor on the fiber scaffold, UV-triggered photocleavage, strand displacement between the walker DNA and the exposed RNA track strand, RNase H cleavage, and translocation.

https://www.sciengine.com/doi/10.1007/s11426-026-3647-6

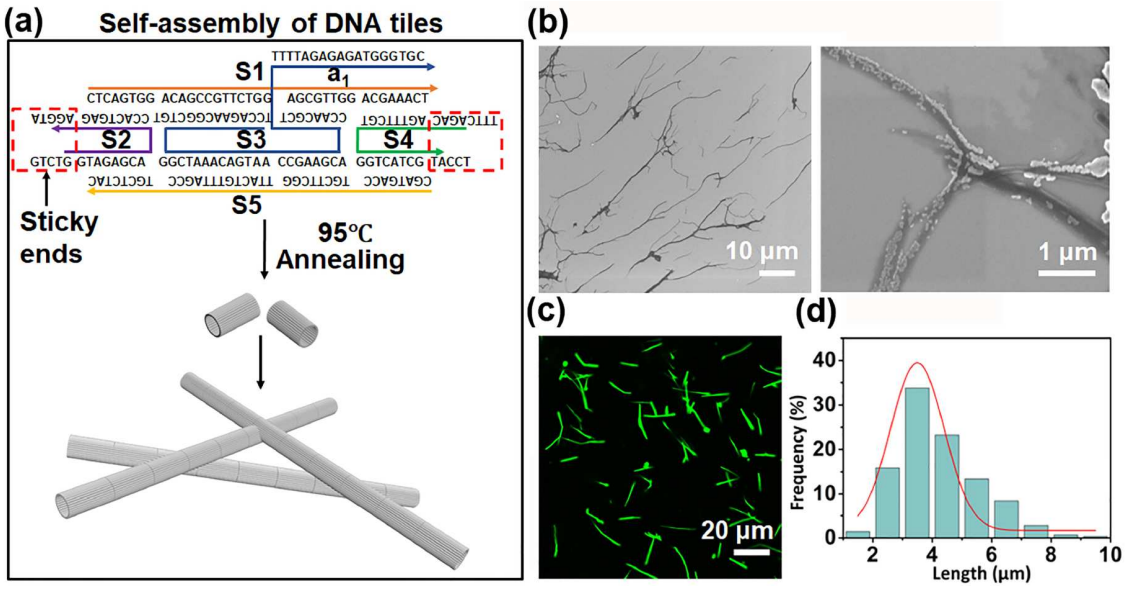

Figure 2 (Color online) Construction and characterization of microscale DNA fiber assemblies based on tile structures. (a) Schematic illustration of the annealing self-assembly process of DNA fiber structures. Five distinct DNA sequences (S1–S5) were subjected to annealing at 95 °C to form tile-like structures, which were further assembled into fiber backbone structures via complementary sticky ends. (b) SEM images reveal the morphology of the self-assembled structures. The left image displays larger structures (scale bar, 10 μm), while the right image is a magnified view of individual structures (scale bar, 1 μm). (c) Fluorescence confocal microscopy imaging of the assembled DNA fiber backbone (scale bar, 20 μm). (d) Length distribution map of DNA fibers.

room temperature. These optimizations ensure that the DNA fibers possess sufficient length, uniform morphology, and good biocompatibility, providing a stable and reliable artificial cytoskeleton for subsequent light-controlled walking and transport. Ultrafiltration was employed to purify the fibers by removing unassembled strands and incomplete tiles, yielding a clean and reproducible scaffold for subsequent experiments (Figure S6).

2.3 Vesicle-based nanomotor transport on DNA fiber assemblies

As depicted in Figure 3a, to mimic intracellular vesicular transport, cholesterol-modified Walker DNA was anchored to SUV (~110 nm diameter, Figure 3b, c). Fluorescence assays confirmed successful functionalization of the SUVs with fluorescence-labeled Walker DNA (Figure 3d). Hybridization between complementary sequences enabled vesicle attachment to the fibers, as visualized by SEM (Figure 3e, f). Mechanistic assays showed that in the absence of RNase H, the fiber scaffold, the track strand, and the walker DNA remained associated together in the same focal plane. Upon addition of RNase H, the fluorescence signals of Cy3 (representing the track strand) and Fam (representing the walker DNA) decreased significantly, indicating that both the track strand and the walker DNA were detached from the fiber scaffold. These results confirm that the hydrolysis of the RNA strand is specifically mediated by RNase H cleavage (Figure S7). Gel assays also showed light-induced hairpin opening and RNase H-dependent cleavage (Figure S8). The DNA modification density on the SUVs was determined to be 1.70×10^5 molecules μm^{-2} by fluorescence quantification (Figure S9). Upon RNase H addition, RNA strands hybridized to the Walker DNA were hydrolyzed, prompting SUV motion along the fiber axis. As the vesicle advanced, the track labeled with Cy3 was cleaved and released, leading to a gradual decrease in fluorescence signal over time (Figure 3g). This rolling mechanism was also successfully applied to inorganic material, such as 15 nm gold nanoparticles functionalized with DNA, confirming the generality of the transport strategy (Figure S10). Cytoskeletal filaments such as microtubules and actin filaments undergo polymerization/depolymerization-driven movement, cortical flow, and even motor protein-mediated translocation. To more comprehensively mimic this dual role, where the cytoskeleton acts both as a track and as a cargo, we further demonstrated that the DNA fibers themselves can serve as movable cargos (Figure S11). The results show the "fuel depletion tracks" (black regions in the Cy3 channel) left behind after the fiber rolling, demonstrating that the fiber itself can serve as a cargo to achieve directional motion. This extension highlights the versatility of our system and its closer analogy to the dynamic behavior of natural cytoskeletons.

2.4 Vesicle motor transport in synthetic cell-like models

To better emulate cellular confinement, all system components were encapsulated within water-in-oil emulsion droplets [44,45]. As shown in Figure 4a, all components necessary for DNA motor rolling were encapsulated into cell-sized droplets using a water-in-oil method. Subsequently, the DNA motors were activated to move along the fibrous skeleton of the synthetic cell-like droplets in the presence of light. Figure 4b, c depicts the morphology of the synthetic cell-like droplets composed of different components. The diameter of the synthetic cell-like droplets was measured to be approximately 7.5 μm, which is comparable to the size of real cells (Figure 4e). In the absence of UV light, the RNA hairpin remained closed, preventing motor activation. UV irradiation cleaved the PC-linker, opening the hairpin and permitting hybridization with the Walker strand. Subsequent RNase H activity induced processive vesicle motion along the fiber, accompanied by cleavage of Cy3-labeled track RNA and a corresponding decrease in fluorescence (Figure 4d, f). Control experiments (without UV irradiation) confirmed that the decrease was primarily caused by RNase H-mediated SUV rolling and cleavage of the track RNA, which released Cy3-labeled track fragments from the fiber scaffold, resulting in a reduced Cy3 signal in the focal plane of the fiber scaffold. Confocal 3D imaging revealed that most of the cleaved Cy3-RNA fragments remained inside the droplets; however, since

https://www.sciengine.com/doi/10.1007/s11426-026-3647-6

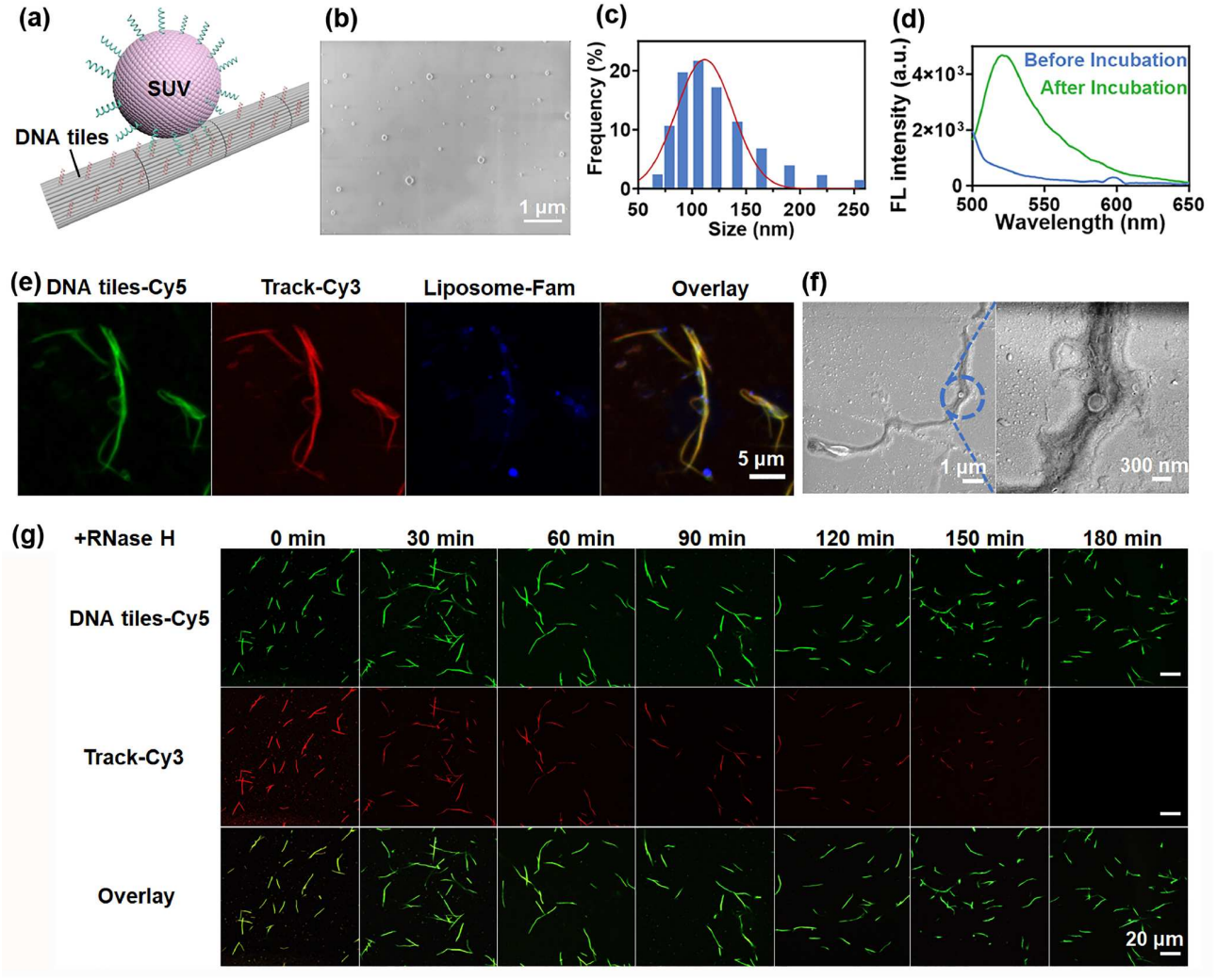

Figure 3 (Color online) Rolling of SUV-based nanomotors on DNA fiber assemblies. (a) Schematic illustration depicting the rolling of SUV motors along the backbone of the DNA fiber. (b) SEM image presenting the morphological features of SUVs (scale bar, 1 μm). (c) Histogram of SUV size distribution reveals that the majority of SUVs are approximately 100 nm in size, indicating a high degree of size homogeneity among the SUVs. (d) Fluorescence spectra showing alterations in fluorescence intensity of SUVs before and after incubation, indicating successful anchoring of cholesterol-modified DNA fragments on SUVs. (e) Fluorescence confocal microscopy images are shown, depicting DNA fiber-Cy5, Track DNA/RNA-Cy3, liposome-Fam, and their corresponding superimposed images (scale bar, 5 μm). (f) SEM images illustrate the binding of SUVs to the DNA fiber backbone (scale bars, 1 & 300 nm). (g) Different time series showing the changes in Cy3 fluorescence under the addition of RNase H, indicating the binding and hydrolysis of DNA motors to the orbital strands on the DNA fiber assemblies, occurring under the catalytic action of RNase H (scale bar, 20 μm).

they were no longer immobilized on the fibers, they appeared as diffuse background signals in confocal scans. Consequently, the fluorescence signal decreased within the quantified regions (*i.e.*, around the fibers). The photobleaching control experiment demonstrated that under intense laser irradiation, Cy3 remained stable and was not susceptible to photobleaching; its fluorescence signal did not change after 600 s of illumination. Therefore, the significant decrease in the Cy3 signal observed in the UV-triggered experiments (at laser intensities lower than that used for photobleaching) cannot be attributed to photobleaching, but rather to RNase H-mediated cleavage of the RNA track. (Figure S12). An alternative synthetic cell design featuring a phospholipid bilayer membrane more closely resembled natural cells but exhibited reduced stability compared to emulsion-based constructs (Figure S13). Further optimization of membrane composition is needed to improve robustness.

2.5 Photocontrol of DNA motors in a single synthetic cell-like droplet

Spatiotemporal control over motor activity was achieved using a confocal microscope equipped with a 405 nm laser for localized UV exposure (Figure 5a). Selective irradiation within defined regions cleaved PC-linkers, activating RNA tracks and initiating motor movement. As motors traversed the illuminated zones, track strands were hydrolyzed and released, leading to a localized reduction in Cy3 fluorescence (Figure 5b, d). Over time, the fluorescence intensity of Cy3 (track) gradually decreased. Moreover, the decrease in Cy3 signal was not uniform but occurred locally and discontinuously along the fiber scaffold, which is consistent with the mechanism of stepwise cleavage of the track RNA as the SUV rolls along the fiber (Figure S14). This approach demonstrates precise, light-directed manipulation of transport within individual synthetic cell-like droplets, highlighting the system's potential for high-resolution operational control.

3 Conclusions

In this study, we have successfully constructed a synthetic bionic cell system in which DNA-based nanomotors execute light-guided directional motion along an artificial cytoskeletal network. This

https://www.scienfine.com/doi/10.1007/s11426-026-3647-6

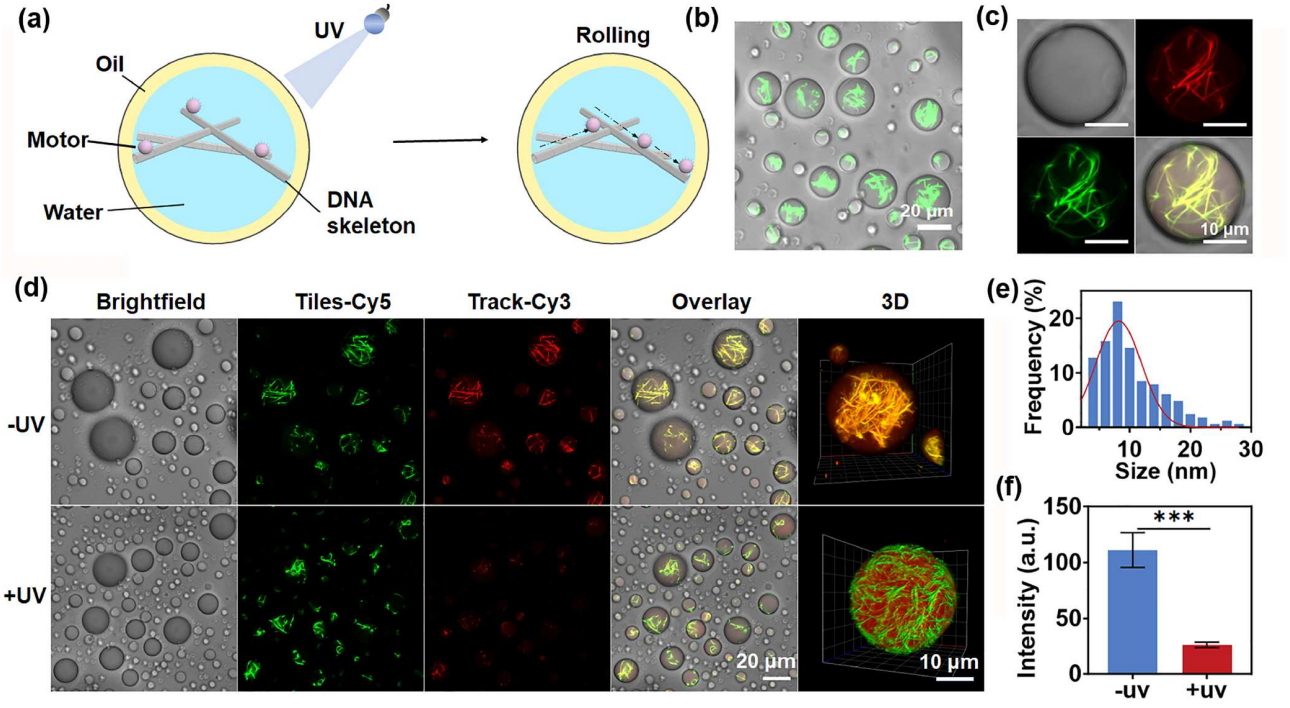

Figure 4 (Color online) Construction of synthetic cell-like droplets using water-in-oil encapsulation. (a) Schematic illustration of the synthetic cell-like model constructed using a water-in-oil encapsulation system. The synthetic cell-like droplet comprises an aqueous phase containing the DNA backbone and DNA motors, surrounded by an oil phase. UV irradiation is employed to activate the DNA motors. (b) Confocal microscopy images showing the morphology of the synthetic cell-like droplets (scale bar, 20 μm). (c) Magnified image of the internal structure of the synthetic cell-like droplet, highlighting detailed features (scale bar, 10 μm; color coding: red, track-pc-Cy3; green, tiles-Cy5). (d) Movement of SUV motors on the synthetic cytoskeleton following UV illumination, which activates the RNA nucleic acid hairpin. Upper and lower panels provide comparative images with and without light treatment, respectively. These include brightfield, Cy5, Cy3, overlay images, and 3D reconstructions (scale bars, 20 & 10 μm). (e) Histogram of structural dimensions. (f) Bar graph comparing the mean fluorescence intensity values (Cy3 channel; Track-pc) between untreated and UV-treated synthetic cell-like droplets. Error bars derived from $n = 10$ droplet samples. The result was obtained by statistical approach of *t*-test analysis. $^{***}P < 0.001$.

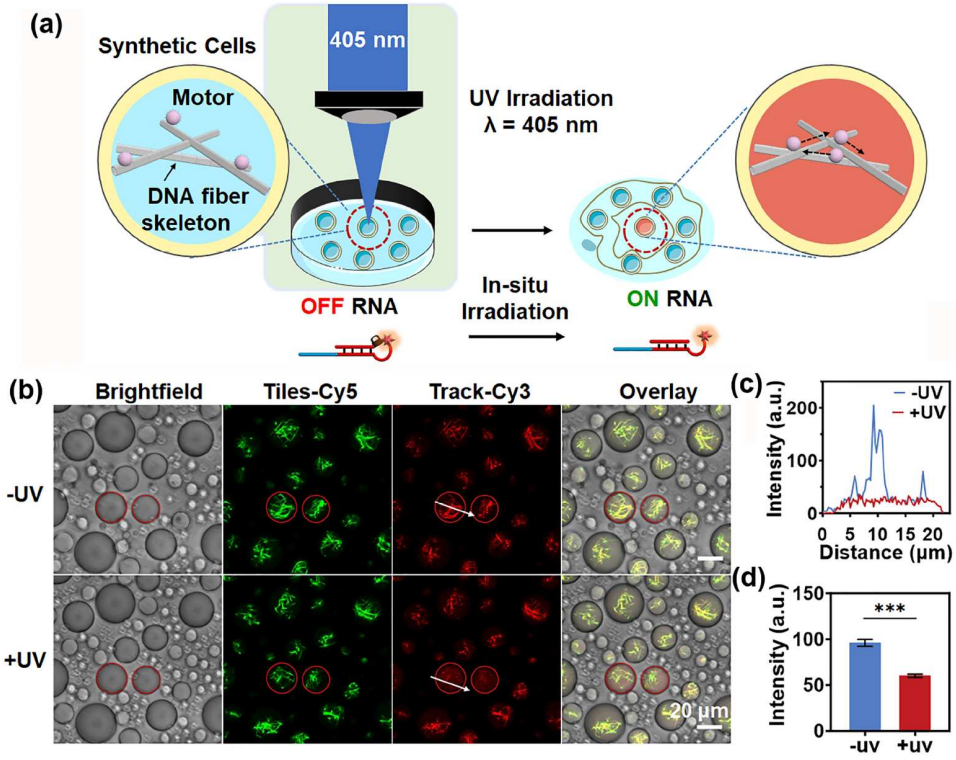

Figure 5 (Color online) *In-situ* photocontrol of DNA motors in single synthetic cell-like droplets. (a) Schematic illustration of the photoactivation process in a single synthetic cell-like droplet. Upon irradiation with 405 nm UV light, the RNA nucleic acid hairpin on the DNA backbone transitions from a closed to an open state, thereby initiating the rolling motion of the DNA motors. (b) Confocal microscopy images depicting localized changes in the artificial cell before and after *in situ* UV irradiation (scale bar, 20 μm). (c) Fluorescence intensity distribution showing the variation in fluorescence intensity with distance in both untreated and UV-treated artificial cells, indicating the release and movement of DNA motors. (d) Bar graph comparing the mean fluorescence intensity values (Cy3 channel; Track-pc) between untreated and UV-treated single droplets, further confirming the hydrolysis of the track strand due to the rolling of DNA motors after UV irradiation. Error bars derived from $n = 3$ droplet samples. The result was obtained by statistical approach of *t*-test analysis. $^{***}P < 0.001$.

http://www.sciencechina.cn/sscp/2026071613128.doc 6277

work integrates the following three functional modules within a cell-sized confined space: (1) a self-assembled DNA fiber scaffold that mimics the cytoskeleton, (2) a photocleavable RNA track that enables spatially on-demand activation, and (3) an RNase H-driven walking mechanism that provides sustained energy for movement. This integration achieves two major breakthroughs over existing systems: first, light-controlled transport with spatial precision down to the single-cell level; second, versatility across multiple cargo types, including lipid vesicles, gold nanoparticles, and even the DNA fibers themselves. These results provide a blueprint for constructing artificial transport systems that more closely resemble natural cells. By integrating precisely designed DNA sequences with photoresponsive elements, we have demonstrated that light can serve as a non-invasive, spatiotemporally precise trigger to regulate motor activity. Our results confirm that the movement of DNA motors on fiber scaffolds is highly controllable and efficient. Through localized UV illumination, we achieved directed motion of motors within individual synthetic cell-like droplets, underscoring the system's spatial resolution and operational accuracy. Emphasis was placed on ensuring the biocompatibility and structural stability of the system by employing biomimetic components such as lipid vesicles, which not only serve as carriers but also enhance the physiological relevance of the model.

Despite these advances, several challenges remain. Future work should focus on enhancing motor performance and loading capacity through structural optimization of DNA components [46,47]. The behavior of DNA motors in more complex and crowded environments-simulating real cellular conditions-also warrants deeper investigation [48,49]. Moreover, the development of advanced real-time imaging techniques will be crucial for tracking motor dynamics and cargo release with high precision [50]. In summary, this work provides a foundational framework for designing functional synthetic cells with programmable transport capabilities, paving the way for innovative applications in synthetic biology and nanomedicine.

Conflict of interest

The authors declare no conflict of interest.

Acknowledgement

This work was supported by the National Natural Science Foundation of China (22377112, 22090050) and the National Key R&D Program of China (2021YFA1200400).

Supporting information

The supporting information is available online at http://chem.scichina.com and http://link.springer.com/journal/11426. The supporting materials are published as submitted, without typesetting or editing. The responsibility for scientific accuracy and content remains entirely with the authors.

References

1 Ringe D, Petsko GA. *Cell*, 2012, 150: 1093–1095
2 Nam W, Epureanu BI. *Phys Rev E*, 2017, 95: 012405
3 Choi D, Go G, Kim D, Lee J, Park S, Di Vizio D, Gho YS. *J Extracell Vesicle*, 2020, 9: 1757209
4 Cortese M, Lee JY, Cerikan B, Neufeldt CJ, Oorschot VMJ, Köhrer S, Hennies J, Schieber NL, Ronchi P, Mizzon G, Romero-Brey I, Santarella-Mellwig R, Schorb M, Boermel M, Mocaer K, Beckwith MS, Templin RM, Gross V, Pape C, Tischer C, Frankish J, Horvat NK, Laketa V, Stanifer M, Boulant S, Ruggieri A, Chatel-Chaix L, Schwab Y, Bartenschlager R. *Cell Host Microbe*, 2020, 28: 853–866.e5
5 Michaelis J, Muschielok A, Andrecka J, Kügel W, Moffitt JR. *Phys Life Rev*, 2009, 6: 250–266
6 Chinappi M, Morozzo della Rocca B. *Nat Nanotechnol*, 2023, 18: 225–226
7 Pradhan B, Kanno T, Umeda Igarashi M, Loke MS, Baaske MD, Wong JSK, Jeppsson K, Björkegren C, Kim E. *Nature*, 2023, 616: 843–848
8 Siti W, Too HL, Anderson T, Liu XR, Loh IY, Wang Z. *Sci Adv*, 2023, 9: eadi8444
9 Cha TG, Pan J, Chen H, Salgado J, Li X, Mao C, Choi JH. *Nat Nanotech*, 2014, 9: 39–43
10 Xu W, Hu F, Li J, Shang J, Liu X, Zeng Y, Wu Q, Wang F. *Sci China Chem*, 2023, 66: 3105–3115
11 Zuo H, Mao C. *Sci China Chem*, 2018, 61: 763–764
12 Mohapatra S, Lin CT, Feng XA, Basu A, Ha T. *Chem Rev*, 2020, 120: 36–78
13 Yin Y, Xiong M, Liu C, Zhang XB, Ou Q. *Sci China Chem*, 2025, 68: 4746–4760
14 Jung C, Allen PB, Ellington AD. *Nat Nanotech*, 2016, 11: 157–163
15 Valero J, Pal N, Dhakal S, Walter NG, Famulok M. *Nat Nanotech*, 2018, 13: 496–503
16 Bazrafshan A, Kyriazi ME, Holt BA, Deng W, Piranej S, Su H, Hu Y, El-Sagheer AH, Brown T, Kwong GA, Kanaras AG, Salaita K. *ACS Nano*, 2021, 15: 8427–8438
17 Ibusuki R, Morishita T, Furuta A, Nakayama S, Yoshio M, Kojima H, Oiwa K, Furuta K'. *Science*, 2022, 375: 1159–1164
18 Harashima T, Otomo A, Iino R. *Nat Commun*, 2025, 16: 729
19 Joseph A, Contini C, Cecchin D, Nyberg S, Ruiz-Perez L, Gaitzsch J, Fullstone G, Tian X, Azizi J, Preston J, Volpe G, Battaglia G. *Sci Adv*, 2017, 3: e1700362
20 Shao J, Cao S, Williams DS, Abdelmohsen LKEA, van Hest JCM. *Angew Chem Int Ed*, 2020, 59: 16918–16925
21 Li H, Gao J, Cao L, Xie X, Fan J, Wang H, Wang H, Nie Z. *Angew Chem Int Ed*, 2021, 60: 26087–26095
22 Pan T, Shi Y, Zhao N, Xiong J, Xiao Y, Xin H, Li B. *Adv Funct Mater*, 2022, 32: 2111038
23 Agarwal S, Klocke MA, Pungchai PE, Franco E. *Nat Commun*, 2021, 12: 3557
24 Arulkumaran N, Singer M, Howorka S, Burns JR. *Nat Commun*, 2023, 14: 1314
25 Burns JR. *Small*, 2021, 17: e2100136
26 Shrivastava A, Du Y, Adepu HK, Li R, Madhvacharyula AS, Swett AA, Choi JH. *ACS Synth Biol*, 2023, 12: 2789–2801
27 Daly ML, Nishi K, Klawa SJ, Hinton KY, Gao Y, Freeman R. *Nat Chem*, 2024, 16: 1229–1239
28 Zhang L, Li Y, Sun J, Zhao Y, Xia F, Huang F, Liu Y, Mao X, Wang S, Zuo X, Han D, Li F, Zhu Z, Qiu L, Li X, Wu X, Chen Y, Yu X, Li S, Zhu W, Li F, Hou J, Yang Q, Wu X, Liu C, Zhang G, Wang Z, Wan W, Yang C, Zhang X, Yang H, Fang X, Tan W. *Sci China Chem*, 2025, 68: 5357–5428
29 Zhan P, Jahnke K, Liu N, Göpfrich K. *Nat Chem*, 2022, 14: 958–963
30 Chen F, Wang D, He L, Liu Y, Du Y, Guo Z, He S, Wang Z, Zhang J, Lyu Y, Tan W. *ACS Nano*, 2023, 17: 6615–6626
31 Ramos Docampo MA, Abild Meyer C, Ryberg C, Otzen DE, Hirsch C, Städler B. *ACS Nano*, 2025, 19: 37324–37338
32 Duan Z, Ouyang Y, Fu Y, Huang F, Xia F, Willner I. *Angew Chem Int Ed*, 2023, 62: e202301476
33 Huang F, Xue H, Fu Y, Ouyang Y, Chen D, Xia F, Willner I. *Adv Funct Mater*, 2023, 33: 2302814
34 Huang F, You M, Han D, Xiong X, Liang H, Tan W. *J Am Chem Soc*, 2013, 135: 7967–7973
35 Liu H, Dong J, Duan Z, Xia F, Willner I, Huang F. *Sci Adv*, 2024, 10: eadp6166
36 Akter M, Moghimianavval H, Luker GD, Liu AP. *Adv Biol*, 2025, 9: e2400539
37 Anderson T, Wu W, Sirbu O, Tong K, Siti W, Rui Liu X, Kou B, Murayama K, Asanuma H, Wang Z. *Angew Chem Int Ed*, 2024, 63: e202405250
38 Lubbe AS, Liu Q, Smith SJ, de Vries JW, Kistemaker JCM, de Vries AH, Faustino I, Meng Z, Szymanski W, Herrmann A, Feringa BL. *J Am Chem Soc*, 2018, 140: 5069–5076
39 Wang Y, Zhang QL, Liu Y, Wang LL, Wu CQ, Shao M, Xing X, Du J, Xu L. *Sci China Chem*, 2025, 68: 694–704
40 Korosec CS, Unksov IN, Surendiran P, Lyttleton R, Curmi PMG, Angstmann CN, Eichhorn R, Linke H, Forde NR. *Nat Commun*, 2024, 15: 1511
41 Yehl K, Mugler A, Vivek S, Liu Y, Zhang Y, Fan M, Weeks ER, Salaita K. *Nat Nanotech*, 2016, 11: 184–190
42 Chen D, Qin Y, Xu S, Xia F, Willner I, Huang F. *Small*, 2025, 21: e2506270
43 Rothemund PWK, Ekani-Nkodo A, Papadakis N, Kumar A, Fygenson DK, Winfree E. *J Am Chem Soc*, 2004, 126: 16344–16352
44 Zhao Q, Cao F, Luo Z, Huck WTS, Deng N. *Angew Chem Int Ed*, 2022, 61: e202117500
45 Liu W, Lupfer C, Samanta A, Sarkar A, Walther A. *J Am Chem Soc*, 2023, 145: 7090–7094
46 Chen Y, Guo Y, Wang J, Liu R, Yang X, Wang K, Pu Y, Shi H, Huang J. *Sci China Chem*, 2024, 67: 2412–2422
47 Pfeiffer M, Cole F, Wang D, Ke Y, Tinnefeld P. *Sci Robot*, 2025, 10: eadu3679
48 Niederholtmeyer H. *Nat Chem*, 2025, 17: 311–313
49 Chen W, Song S, Samanta A, Sethi S, Drees C, Kappl M, Butt HJ, Walther A. *Nat Chem Eng*, 2025, 2: 627–639
50 Lee J, Chen LF, Gaudin S, Gupta K, Novacic A, Spakowitz A, Boettiger AN. *Science*, 2025, 389: eadx2202

https://www.sciengine.com/doi/10.1007/s11426-026-3647-6